Epitaxial mosaic-like Mn5Ge3 thin films on Ge(001) substrates

Adriana Alvídrez-Lechuga, Ricardo López Antón, Luis Fuentes-Cobas, José Holguín-Momaca, Óscar Solís-Canto, Francisco Espinosa-Magaña, Sion Olive-Méndez

Epitaxial mosaic-like Mn_5Ge_3 thin films on Ge(001) substrates

Adriana Alvídrez-Lechuga[1], Ricardo López Antón[2], Luis E. Fuentes-Cobas[1], José T. Holguín-Momaca[1], Óscar O. Solís-Canto[1], Francisco Espinosa-Magaña[1], and Sion F. Olive-Méndez[1,*]

[1]*Centro de Investigación en Materiales Avanzados, S.C. (CIMAV), Miguel de Cervantes 120, C.P. 31136, Chihuahua, Chih., Mexico.*

[2]*Instituto Regional de Investigación Científica Aplicada (IRICA) and Departamento de Física Aplicada, Universidad de Castilla-La Mancha, 13071, Ciudad Real, Spain.*

Email: sion.olive@cimav.edu.mx

Abstract

Epitaxial mosaic-like Mn_5Ge_3 thin films were grown on Ge(001) substrates using reactive deposition epitaxy process from Mn deposition or Mn-Ge co-deposition at a substrate temperature of 250 °C using magnetron sputtering. The cross-sectional transmission electronic microscopy analyses reveal an abrupt interface at the atomic scale; two equivalent epitaxial relationships are found between the substrate and the Mn_5Ge_3 crystallites: Ge(001)[110] and $[1\bar{1}0]$ ∥ $Mn_5Ge_3(1\bar{1}1)[\bar{1}\bar{1}0]$. The c_{hex} axis of Mn_5Ge_3 forms an angle of 45° with the substrate plane. Rietveld analysis from a synchrotron 2-dimensional diffraction pattern revealed that remanent deformations of about 1% exist in the film. *M-H* measurements of 50-nm thick films elaborated by co-deposition revealed a saturation magnetization, M_s, of 636 kAm^{-1}, whereas the films elaborated by Mn deposition saturate at different values depending on the orientation of the applied magnetic field: $M_s^{\perp}$=545 kAm^{-1} and $M_s^{\parallel}$=774 kAm^{-1}. This M_s difference is attributed to shape anisotropy of crystallites and interface quality of the films.

Keywords: Mn_5Ge_3; Ge(001); epitaxy; sputtering; synchrotron; magnetic properties.

1 Introduction

Spintronics, unlike traditional electronics, offers faster data processing and lower power consumption [1], among other advantages as non-volatile data storage [2,3]. The spin field effect transistor (spin-FET) is one of the most promising spintronic devices, which allows data processing at the same time that information can be stored within the magnetic orientation of the emitter and collector in order to manipulate the input and output of the transistor [4]. One of the requirements for the fabrication of a spin-FET is the selection of a suitable material for the emitter, which will take the role of an efficient ferromagnetic (FM) spin injector [5]. Diluted magnetic semiconductors (DMS) allow spin injection with an efficiency of ~ 10% at around 40 K. However, the use of DMS is limited due to their low Curie temperature (T_C) [6]. Additionally, it is difficult to preserve the spin polarization in a FM/insulator/semiconductor multilayer heterostructure due to the multiples interfaces that produce a loss of spin coherence. A heterostructure that provides a better approach for an efficient spin injection is a FM/semiconductor multilayer with a Schottky barrier at the interface [7]. For this purpose, Mn_5Ge_3 has become an important material for its FM ordering with a T_C = 296 K and polarization above 42% [8,9]. The hexagonal crystal structure $P6_3/mcm$ of Mn_5Ge_3 has lattice parameters $a = b = 7.184$ Å and $c = 5.053$ Å [10], which allows the growth on Ge(111) substrates within a lattice mismatch of 3.7%. Mn_5Ge_3 can be easily synthesized as a continuous thin film on Ge(111) using molecular beam epitaxy (MBE) technique. The epitaxial relationship is Ge(111)[110] ∥ Mn_5Ge_3(001)[100] [11]. However, the development of these structures is not suitable for the microelectronic industry, since Ge(111) is not compatible with the Si(001) technology used in most of the microelectronic devices. Ge(001)/Mn_5Ge_3 heterostructures offer the possibility of integration of an efficient spin injector into the Si(001) technology [12,13]. Recent studies of Mn_5Ge_3 thin films grown on Ge(111) substrates demonstrate that the easy axis of magnetization lies on the basal (001) plane for films with thickness <25 nm, while the hard axis of magnetization lies along the *c* axis (oppositely to the bulk properties where the *c* axis is the easy axis) [14]. It has been observed that the magnetic anisotropy is directly related to the thickness of the films, as the thickness increases the easy axis turns progressively out the basal plane, but it never becomes perpendicular to the film plane [15,16,17].

The growth of Mn_5Ge_3 on Ge(001) substrates using the solid phase epitaxy (SPE) method [18], which consists on Mn deposition at room temperature (RT) followed by thermal annealing, produces randomly distributed Mn_5Ge_3(001) nanoislands with average diameters of 80 nm and heights of 20 nm [19,20]. Thus another growth process needs to be considered to obtain thin films. Dang et al. [21] elaborated Mn_5Ge_3 thin films by MBE using reaction deposition epitaxy (RDE) method, consisting on the deposition of Mn or co-deposition of Mn and Ge at a substrate temperature, T_s, higher than RT. The thin films were grown by Mn and Ge co-deposition at 150 °C on GaSb(001) and GaAs(001) substrates. The obtained T_C were 350 and 320 K. The epitaxial relationships were identified as GaAs(001) ‖ Mn_5Ge_3(111) and GaSb(001) ‖ Mn_5Ge_3(111), respectively. In this work we have found a similar epitaxial relationship between Mn_5Ge_3 and Ge(001) but instead of the (111) plane is the $Mn_5Ge_3(1\bar{1}1)$ plane that is parallel to the Ge(001) surface within an angle of 6°.

Furthermore, doping Mn_5Ge_3 with carbon allows an increase of T_C up to ~ 450 K, due to a modification of the electronic structure [22,23,24]. Carbon doping increases the thermal stability of the compound and suppresses the segregation of Mn towards further deposited layers, in particular Ge [25,26]. For these reasons C-doped Mn_5Ge_3 is a promising candidate to be used as a spin injector on IV-group semiconductors.

In this paper, we report the growth of Mn_5Ge_3 thin films on Ge(001) substrates employing the RDE method. The thin film crystal growth obeys to a Stranski-Krastanov growth mode. The analyses performed by transmission electron microscopy show epitaxially grown crystallites with a sharp interface with the substrate and two epitaxial relationships. In-plane (IP) and out-of-plane (OP) magnetic *M-H* measurements revealed an IP easy axis of magnetization.

2 Experimental methods

a) *Experimental setup*

Epitaxial layers were grown in a sputtering system equipped with a reflection high-energy electron diffraction system (RHEED) from STAIB operating at 30 kV to control the morphology and the crystalline structure of the sample surface. A quartz balance is used to measure the deposition rate of Mn and Ge at different powers, which was previously

calibrated by depositing thin films with nominal thicknesses and then measured by scanning electron microscopy. The growth chamber has a base pressure better than 5×10^{-8} Torr and the atomic flux sources are two 2-inch high-purity 99.99% Mn and Ge targets eroded at 45 and 30 W with growth rates of 1.4 and 1.2 nm/min, respectively. Thin films were elaborated by direct deposition of Mn or by co-deposition with Ge. The operating Ar pressure is 3 mTorr, and sputtering was achieved using radio-frequency power sources. Supplemental structural characterization of the investigated sample was performed by grazing-incidence two-dimensional x-ray diffraction (GI-2D-XRD) at beamline 11-3 of the Stanford Synchrotron Radiation Lightsource (SSRL). Grazing incidence experiments take advantage of the relatively large surface area bathed by the x-rays. Applied wavelength was λ = 0.97354 Å. Measurements were accomplished with a mar345 detector. The experimental setup was calibrated with a LaB_6 standard. The sample-detector distance was of 125 mm; pixel and spot linear dimensions were of 0.1 mm and incidence angle was 1°. One-dimensional (1D) pattern was obtained by integration of the Debye rings, processed by the software FIT2D [27]. Atomic force microscopy (AFM) images were obtained with a Veeco SPM MultiMode equipment in tapping mode. The transmission electron microscopy (TEM) sample preparation in cross-section was carried out using a focused ion beam (FIB) with a JEOL JEM-9320FIB equipment. The high-resolution (HR-TEM) images were acquired in scanning-TEM (STEM) mode with a JEOL JEM 2200Fs + Cs equipment operating at 200 kV. Finally, *M-H* and *M-T* curves were obtained with a superconducting quantum interference device (SQUID) from Quantum Design.

b) *Surface preparation*

Prior to the thin film growth on Ge(001) substrates, an *ex-situ* substrate cleaning was carried out. *N*-type Ge(001) sections of 1×1 cm^2 were first wet chemical cleaned by sonication for 20 min using trichloroethylene, acetone and ethanol and deionized water after each solvent bath. A sample substrate was then introduced into the growth chamber through a load lock chamber. The RHEED pattern at this stage shown in Fig. 1(a) consists on a 1×1 ordered strikes corresponding to a non-reconstructed surface, as the GeO_2 native oxide is still present on the sample surface. The sample is then subjected to an *in-situ* cleaning. The first step is a thermal degassing at 400 °C for 4 h and second, a surface

etching with an Ar-biased plasma at the sample holder with a power of 40 W for 20 min at RT to remove remaining C-based molecules and the native GeO_2 layer. The result is an amorphous surface, which RHEED patterns consists only of a continuous background as depicted in Fig. 1(b). Finally, to induce crystalline order at the surface of the sample, a rapid thermal annealing at 700 °C for a few minutes is performed until a 2×1 reconstructed surface is observed by RHEED as shown in Fig. 1(c). The sample is then cooled slowly to 250 °C to perform crystal growth. Mn_5Ge_3 thin films were grown following two different approaches: 1) Direct Mn deposition on Ge(001) substrate and 2) Mn and Ge co-deposition at stoichiometric calibrated fluxes to match the Mn_5Ge_3 composition. The used method for the film growth in both cases is RDE with T_s = 250 °C. This temperature is selected as it is higher than the initiation temperature, T_i, at which the reaction between Mn and Ge takes place to form Mn_5Ge_3 [28], but lower enough to avoid the formation of the $Mn_{11}Ge_8$ phase [29]. In the case of Mn and Ge co-deposition, only local diffusion is required so Mn and Ge atoms find the most convenient position minimizing the surface free energy and the interface free energy of the layer upon the experimental conditions, i.e., T_s = 250 °C.

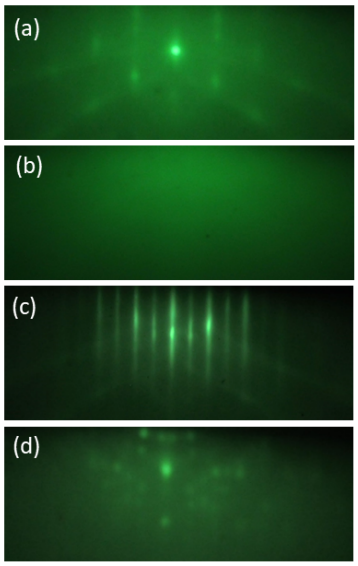

Figure 1. RHEED patterns of the substrate cleaning process and the thin film growth. (a) 1×1 ordered strikes corresponding to a non-reconstructed surface. (b) Amorphous surface after plasma etching. (c) 2×1 reconstructed surface. (d) Initial steps of the Mn_5Ge_3 growth.

3 Results and discussion

The RHEED pattern at the initial steps of the thin film growth (thickness of 5 nm) is shown in Fig. 1(d), the ordered signal is lost rapidly as the thickness of the layer increases due to the beam dispersion and to the high RMS roughness of the surface. The spots on the RHEED diffraction pattern indicate electron diffraction on transmission mode due to the high roughness of the surface. Nevertheless, one can note certain symmetry of the obtained spots along the principal specular spot indicating a good crystalline quality of the film. The evolution of the morphology of the surface (measured by atomic force microscopy) for different thicknesses is shown in Figs. 2(a)-2(d) for Mn deposition and in Figs. 2(e)-2(h) for Mn and Ge co-deposition.

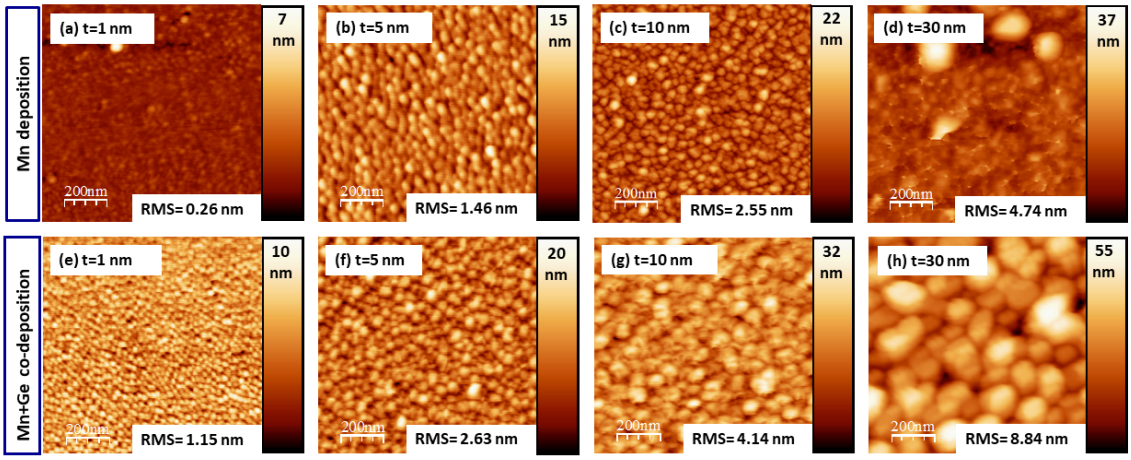

Figure 2. AFM micrographs of Mn_5Ge_3 thin films with different thicknesses (t) grown at T_s = 250 °C by Mn deposition (a)-(d) and by Mn and Ge co-deposition (e)-(h). Both growth approaches follow the Stranski-Krastanov growth mode.

The evaluation of the RMS roughness and the z-scale is an indication that 3-dimensional growth takes place for both approaches. However, by co-deposition it seems that coalescence and/or surface diffusion plays a major role as the grain size increases with the film thickness and hence its RMS roughness. For example, for a thickness of 1 nm, the RMS roughness is 1.15 nm. Meanwhile, the roughness for a film obtained by Mn deposition with a thickness of 1 nm is 0.26 nm, which is equal to the RMS roughness of a

bare substrate, indicating that a wetting layer is perfectly formed over the substrate followed by a 3-dimensional growth. In both cases, the wetting layer covers the Ge surface completely, but Mn deposition leads to a more ordered growth regarding the morphology of the layer (i.e., more close to a layer-by-layer growth). In both cases a Stranski-Krastanov growth mode takes place.

To examine the crystalline nature of the film, HR-TEM experiments were performed on numerous samples with a thickness of 50 nm elaborated by both approaches Mn-deposition and co-deposition of Mn and Ge. Due to the similarity of the samples grown by Mn deposition and co-deposition, in figure 3(a) is shown a HR-TEM micrograph of a representative region of the Mn_5Ge_3 thin film grown by co-deposition of Mn and Ge. The image shows an epitaxial growth of Mn_5Ge_3 on Ge(001) substrate exhibiting an abrupt interface, as required for efficient spin injection. The interatomic distance of 6.74 Å is close to 6.22 Å which is the projection of the lattice parameter a = 7.184 Å along the $[1\bar{1}0]$ direction of Mn_5Ge_3 ($6.22 = 7.184 cos 30°$). The higher value indicates a tensile deformation of about 8.3% near the interface. Distortions up to 10.2% and without the formation of misfit dislocations have been observed on Mn_5Ge_3 nanoislands epitaxially grown on Ge(001) [19]. The interplanar distance of 4.80 Å matches the interplanar distance along the c axis, which is 5.053 Å, with a compressive deformation of -5%. Both distances allow the identification of the c_{hex} axis [001] direction of Mn_5Ge_3 to form an angle of 45° with the substrate plane. A similar angle has been reported on nanoclusters of Mn_5Ge_3 embedded in a highly diluted Ge:Mn matrix [30].

The Fig. 3(b) shows a HR-TEM image, corresponding to another region of the same sample (i.e., a different region than that shown in Fig. 3(a)). The atomic rows that are perpendicular to the interface correspond to either (100) or (010) atomic planes; their periodicity, measured within the resolution of the line profile scan of the HR-TEM micrograph, is 5.95 Å against 6.22 Å for the bulk lattice constants. Here is important to note that the atomic periodicity of Ge atoms along the $[\bar{1}\bar{1}0]$ direction is 4 Å, which implies that 3 Ge cells match with 2 Mn_5Ge_3 cells. Thus the appropriate interatomic distance should be 6 Å instead of 5.95 Å measured upon the resolution of the line profile scan. Along with this direction, the lattice mismatch is 5.22% calculated from the expression $\Delta a/a = (a_{\mathrm{film}} - a_{\mathrm{sub}})/a_{\mathrm{sub}}$

where *a* stands for the lattice parameter and the subscript indicates if it corresponds to the film or the substrate.

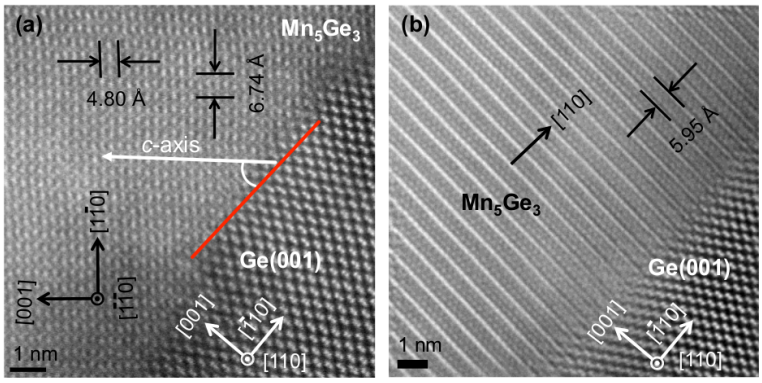

Figure 3. HR-TEM micrographs of a Ge(001)/Mn_5Ge_3 epitaxial mosaique-like thin film grown by Mn and Ge co-deposition at 250 °C showing the (a) Ge(001)[110] ‖ $Mn_5Ge_3(1\bar{1}1)[\bar{1}\bar{1}0]$ and (b) Ge(001)[$1\bar{1}0$] ‖ $Mn_5Ge_3(1\bar{1}1)[\bar{1}\bar{1}0]$ epitaxial relationships.

In this case, the parallel directions between the film and the substrate are Ge[$1\bar{1}0$] ‖ $Mn_5Ge_3[\bar{1}\bar{1}0]$ compared to Ge[110] ‖ $Mn_5Ge_3[\bar{1}\bar{1}0]$ of the previous HR-TEM micrograph. The conclusion to this point is that the film is composed of epitaxial crystallites forming a mosaic-like microstructure. Each crystallite is observed as a single grain in the AFM micrograph in Fig. 2(h), each crystallite has its epitaxial relationship where the difference between the orientation of two crystallites is a simple rotation of 90° in agreement with the four-fold symmetry of the substrate.

To find the plane of Mn_5Ge_3 that is parallel to the substrate surface, we simulate the crystalline structure of Mn_5Ge_3 based on the HR-TEM observations. Figures 4(a) and 4(b) show the projection of the crystalline structure in a side and top view, respectively. The side view of the unit cell shows that four atomic planes are stacked along the *c* axis. The planes $z = 0$ and $z = 1/2$ contain only Mn atoms (denoted as Mn-I) while the planes $z = 1/4$ and $z = 3/4$ contain Mn-II and Ge atoms in equal amounts forming a Mn-Ge layer [31]. To better understand the epitaxial relationship from the HR-TEM micrographs, in Fig. 4(c) is shown a diagram indicating that the $Mn_5Ge_3(1\bar{1}1)$ plane with an additional anticlockwise rotation of 6° is required to match the Ge(001) plane. The complete epitaxial relationship,

including the two perpendicular directions of the Ge(001) substrate is Ge(001)[110] and $[1\bar{1}0]$ ‖ $Mn_5Ge_3(1\bar{1}1)[\bar{1}\bar{1}0]$. Several epitaxial relationships were found on the growth of Mn_5Ge_3 nanoclusters embedded in a Ge matrix, suggesting that different orientations of the c_{hex} axis can be manipulated depending on the growth parameters and selected substrate [30]. However, the most common epitaxial relationship between embedded clusters [32] or endotaxially [33] grown Mn_5Ge_3 nanoislands [19] is Ge(001)[110] ‖ $Mn_5Ge_3(001)[110]$.

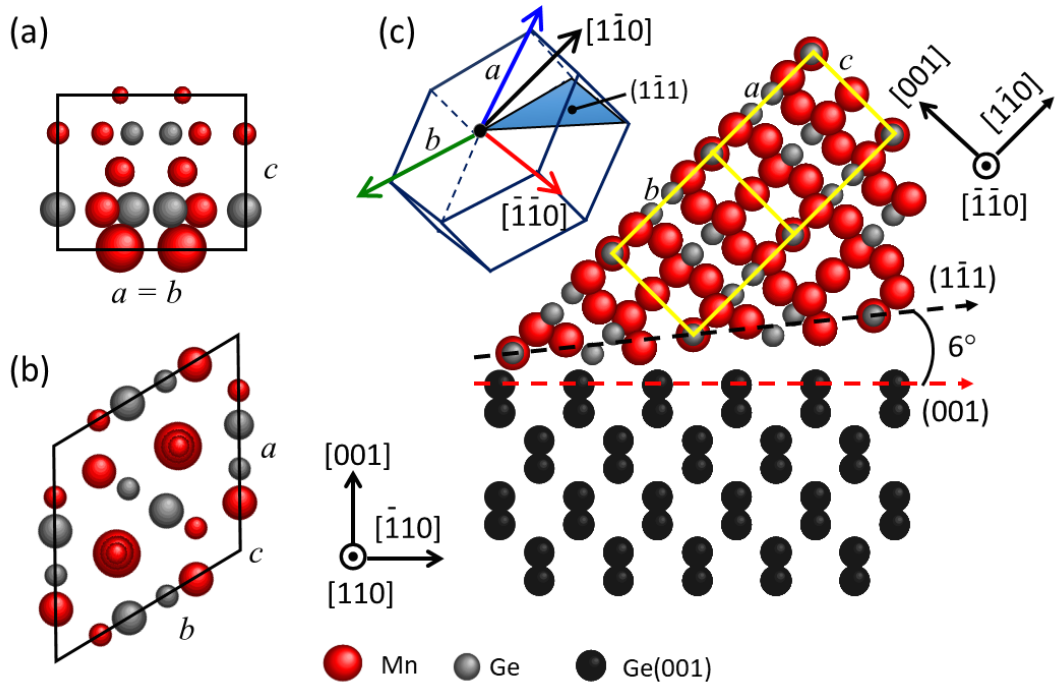

Figure 4. Simulated diagram of the Mn_5Ge_3 compound. (a) Side view (b) and top view. (c) Diagram depicting the epitaxial relationship Ge(001)[110] ‖ $Mn_5Ge_3(1\bar{1}1)[\bar{1}\bar{1}0]$. The $Mn_5Ge_3(1\bar{1}1)$ plane matches the Ge(001) plane within an anticlockwise rotation of 6°.

Theoretical calculations of the interface energy of different Mn_5Ge_3-Ge systems show that the interface energy of the heterostructure of Ge(111)/Mn_5Ge_3(001) is 35 meV/Å^2, whereas the interface energy of Ge(001)/Mn_5Ge_3(001) is 87 meV/Å^2 [34], which is less stable than the films grown on Ge(111). Therefore, in our samples, the *c* axis rotates 45° to minimize the interface energy and to match the lattice parameter of the substrate.

Figure 5(a) shows the result of the GI-2D-XRD experiment with a sample elaborated by co-deposition. The diffraction pattern consists of discontinuous rings attributed to hexagonal crystallites forming an axially-symmetric texture. Axial texture corresponds to a columnar morphology in agreement with the mosaic-like microstructure described before. Sputtering processes also induce columnar growth, so conditions for axial texture are highly favorable. Figure 5(b) shows the 1D-XRD pattern obtained from the two-dimensional one, with its Rietveld refinement via Le Bail profile matching with R-factors: Rp = 5.92, Rwp = 7.47 and χ^2 = 8.54. Peaks' broadening in Figure 5(b) is apparent. The principal sources of peak broadening are small crystal size, nonuniform microstrains and instrumental broadening. The AFM images allowed the measurement of crystallite size, which is approximately 37 nm. Instrumental broadening is known from the setup calibration. The representation of the cell dimensions physical microstrains via lattice parameters uncertainties are a = 7.26(8) Å and c = 5.08(6) Å (bulk lattice parameters are $a = b$ = 7.184 Å and c = 5.053 Å), angles between a, b and c axes remain unchanged. XRD result for crystallite size was 29 nm, close enough to the electron microscopy value.

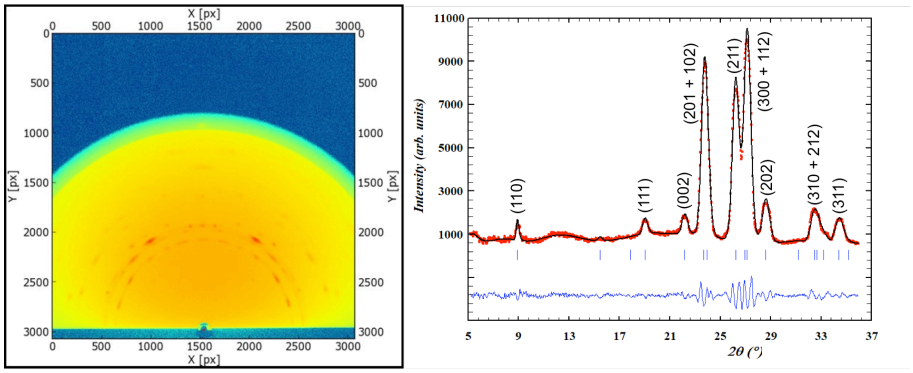

Figure 5. (a) Two-dimensional and (b) one-dimensional synchrotron x-ray diffraction patterns. Peaks' broadening leads to nonuniform microstrains measurement via Rietveld profile matching analysis.

With crystallite size and instrumental broadenings taken into account, Rietveld analysis allowed estimating sample's nonuniform microstrains as roughly 1%. This value is an average over a volume that includes Mn_5Ge_3 and the Mn_5Ge_3–Ge interface. The

deformations at the interface, as measured from the HR-TEM micrographs, are naturally larger.

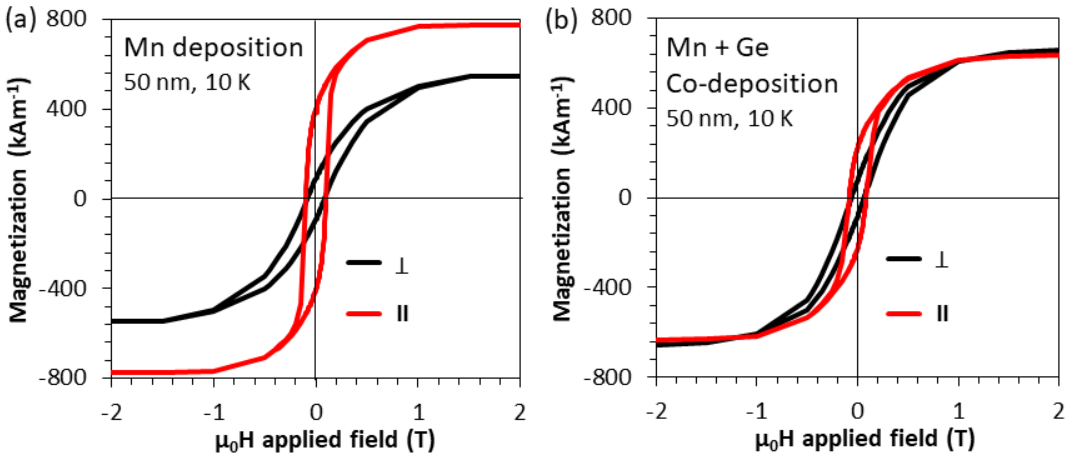

Figure 6. In-plane and out-of-plane *M-H* loops of samples grown by (a) direct deposition of Mn and (b) co-deposition of Mn and Ge.

The magnetic properties of the 50-nm-thick films elaborated by the two different approaches have been examined by SQUID magnetometry. In Figs. 6(a) and 6(b) are shown the IP and OP *M-H* loops at 10 K of the samples grown by Mn deposition and Mn-Ge co-deposition, respectively. The fact that IP and OP anisotropies (hysteresis on the *M-H* loops) are present simultaneously in both films is attributed to the 45° angle between the *c* axis and the normal of the film. However, the IP and OP anisotropies are not equal, nor in the Mn-Ge co-deposition sample neither on the Mn-deposition sample. Remanent magnetization (M_r) is higher on the IP *M-H* measurements, saturation magnetization (M_s) is also reached faster (at lower magnetic fields) in the IP *M-H* loops than in the case of the OP *M-H* curves, indicating that the film plane behaves as an easy magnetization plane, and the normal of the film as the hard axis of magnetization. For the normalized loops (not shown) $M_r = 0.5M_s$ for the Mn-deposition sample while for the sample elaborated from Mn and Ge co-deposition $M_r = 0.39M_s$. This difference is attributed to the interface extension (few atomic layers) and crystalline quality of the film. There is a clear difference on the growth mechanism of both films: while the Mn and Ge co-deposition sample has a Mn_5Ge_3 growth front obeying a Stranski-Krastanov growth mode, the film grown by Mn deposition is

created additionally by Ge and Mn atomic diffusion. Therefore, the interface quality and the magnetic behavior of the film at the interface should be different, as it is evidenced by the differences in the shape of the *M-H* loops. Another significant difference between both samples are the different values of M_s. In the co-deposited layer, saturation reaches the same values in both IP and OP directions, M_s=636 kAm^{-1} while different values of M_s are obtained on the layer elaborated by Mn deposition: $M_S^{\perp}$=545 kAm^{-1} and $M_S^{\parallel}$=774 kAm^{-1}. This kind of discrepancy between the $M_S^{\perp}$ and $M_S^{\parallel}$ have related sometimes in the literature to compressive deformations [35,36]. However, in our case the deformation found is about 1 %, which does not seem enough to explain such a behavior. It is possible that this latest sample possesses a better interface crystalline quality and that the magnetic domains may be preferentially extended along the film plane and by the effect of shape anisotropy of single crystallites the value of $M_S^{\parallel}$ is larger than $M_S^{\perp}$ as a larger demagnetizing field may take place on the OP magnetization measurement. It has been proposed that the magnetic domains in Ge(111)/Mn_5Ge_3 thin films, where the *c* axis is perpendicular to the film plane, consist of stripes for critical thicknesses under 25 nm. Thicker films exhibit additionally OP oriented domains located between IP magnetic domains, which favor the OP anisotropy [14]. In our samples the *c* axis is turned towards the plane of the film by 45º and it cannot be neglected the existence of both orientation of the magnetic domains (parallel and perpendicular to the film plane). But, nevertheless, the magnetic measurements seem to indicate that IP anisotropy is favored (more notably on the samples elaborated by Mn deposition). This issue reinforces the proposed feature that IP plane domains are elongated in the film plane and the conjunction of the effect of shape anisotropy produces a higher value of $M_S^{\parallel}$. Furthermore, in the film elaborated from the Mn deposition, the thin film growth is closer to a layer-by-layer growth at the initial growth stages. This is pinpointed by the lower RMS roughness values for all samples obtained by Mn deposition than those of the Mn-Ge co-deposited samples, indicating a more ordered crystal growth in agreement with the supposition of a higher interface crystalline quality.

Figure 7 shows the magnetization dependence on the temperature *M-T* curves for both samples measured along the plane of the film. The behavior of the film is completely FM with a decrease of magnetization by increasing the temperature. To accurately measure the T_C a fit has been performed according to the model:

$$m(\tau) = \left[1 - s\tau^{3/2} - (1-s)\tau^{p}\right]^{1/3}, \quad (1)$$

where $\tau = T/T_C$, $s > 0$ and $p > 3/2$ are parameters [37]. The fits for both samples are shown as solid black lines in Fig. 7 that exactly match the shape of the experimental curves. The corresponding T_C is 305 K for both samples, which is scarcely larger than the value of 296 K usually reported [10]. A similar increase of T_C has been found by Dang et al. [21] on the growth of Mn_5Ge_3 thin films on GaSb(001) (T_C = 320 K) and GaAs(001) (T_C = 350 K) substrates with compressive lattice mismatches of ~ -9.5% and ~ -1.3%, respectively. The authors propose that the lattice mismatch, and hence the induced deformation, is at the origin of the enhancement of T_C. In our experiments the final remanent deformation of circa 1 % calculated from the Rietveld analysis is not large enough to produce such a significant increase on the T_C as in the case of Mn_5Ge_3 nanoislands where an induced tensile deformation of 10% leads to an increase of T_C up to 350 K [19].

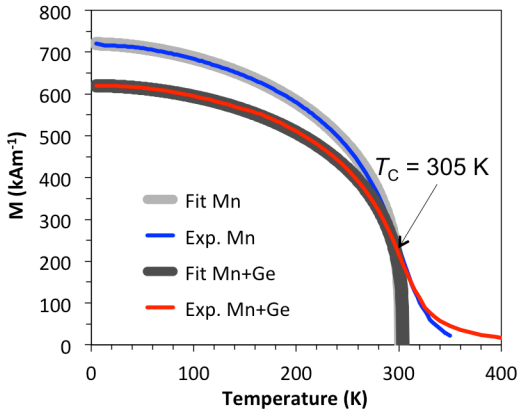

Figure 7. M-T curves of the samples grown by Mn deposition and Mn-Ge co-deposition.

Conclusions

We have obtained epitaxial mosaic-like Mn_5Ge_3 thin films on Ge(001) substrates using the RDE method through Mn deposition and co-deposition of Mn and Ge at a T_s = 250 °C by magnetron sputtering technique. Thin films grown by co-deposition of Mn and Ge showed a higher roughness than the samples grown by Mn deposition while a roughness equal to that of the substrate is obtained on ultrathin films, concluding that a wetting layer has been formed at the initial growth steps. The growth is then followed by an island-like growth;

this process corresponds to a Stranski-Krastanov growth mode. The obtained epitaxial relationship is Ge(001)[110] ‖ $Mn_5Ge_3(1\bar{1}1)[\bar{1}\bar{1}0]$, where the c_{hex} axis [001] of Mn_5Ge_3 forms an angle of 45° with the substrate plane and the plane $(1\bar{1}1)$ of Mn_5Ge_3 forms an angle of 6° with the Ge(001) plane. Rietveld analysis from the synchrotron x-ray diffraction patterns revealed that micro tensions remain in the film with a deformation of 1%. The SQUID *M-H* measurements show that the films obtained by co-deposition exhibit an in-plane and out-of-plane magnetization of 636 kAm^{-1}, whereas the thin films obtained by deposition of Mn show a $M_S^{\perp}$=545 kAm^{-1} and $M_S^{\parallel}$=774 kAm^{-1}. The reason of the enhancement of the in-plane $M_S^{\parallel}$ is attributed to shape anisotropy of single crystallites of Mn_5Ge_3. Finally, the Curie temperature has been enhanced to 305 K due to the effect of residual microtensions.

Acknowledgments

The authors thank the financial support received from Ciencia-Básica SEP-CONACYT grant No. 157559, Fondo Mixto Chihuahua FOMIX No. CHIH-2011-C03-168831 and from the Spanish MINECO (project MAT2014-58034-R) and JCCM (project PEII-2014-042-P). They also thank Carlos Elías Ornelas-Gutiérrez for HR-TEM observations, and the facilities from Laboratorio Nacional de Nanotecnología and from the Stanford Synchrotron Radiation Lightsource, where the 2D-XRD measurements were performed.

References

[1] Y. Saito, T. Marukame, T. Inokuchi, M. Ishikawa, H. Sugiyama, T. Tanamoto, Spin injection, transport, and read/write operation in spin-based MOSFET, Thin Solid Films 519 (2011) 8266–8273.

[2] W.S. Zhao, T. Devolder, Y. Lakys, J.O. Klein, C. Chappert, P. Mazoyer, Design considerations and strategies for high-reliable STT-MRAM, Microelectronics Reliability 51 (2011) 1454–1458.

[3] T. Kawahara, K. Ito, R. Takemura, H. Ohno, Spin-transfer torque RAM technology: Review and prospect, Microelectronics Reliability 52 (2012) 613–627.

[4] S. Das Sarma, Spintronics: A new class of device based on the quantum of electron spin, rather than on charge, may yield the next generation of microelectronics, American Scientist, 89 (2001) 516-523.

[5] I.A. Fischer, J. Gebauer, E. Rolseth, P. Winkel, L.-T. Chang, K.L. Wang, C. Sürgers, J. Schulze, Ferromagnetic $Mn_5Ge_3C_{0.8}$ contacts on Ge: work function and specific contact resistivity, Semicond. Sci. Technol. 28 (2013) 125002.

[6] A. Gabel. Spintronics: The problem of efficient polarized spin injection. Introduction to solid-state physics. *Boston University*.

[7] S. Olive-Mendez, A. Spiesser, L.A. Michez, V. Le Thanh, A. Glachant, J. Derrien, T. Devillers, A. Barski, M. Jamet, Epitaxial growth of Mn_5Ge_3/Ge(111) heterostructures for spin injection, Thin Solid Films 517 (2008) 191–196.

[8] R.P. Panguluri, C. Zeng, H.H. Weitering, J. M. Sullivan, S.C. Erwin, B. Nadgorny, Spin polarization and electronic structure of ferromagnetic Mn_5Ge_3 epilayers, Phys. Stat. Sol. (B) 242 (2005) R67–R69.

[9] H.K. Yuan, H. Chen, A.L. Kuang, C.L. Tian, J.Z. Wang, Electronic structural and magnetic properties of Mn_5Ge_3 clusters, J. Chem. Phys. 139 (2013) 204307.

[10] C. Zeng, S.C. Erwin, L.C. Feldman, A.P. Li, R. Jin, Y. Song, J.R. Thompson, H.H. Weitering, Epitaxial ferromagnetic Mn_5Ge_3 on Ge (111), Appl. Phys. Lett. 83 (2003) 5002-5004.

[11] L.-J. Chen, D.-Y. Wang, Q.-F. Zhan, W. He, Q.-A. Li, Z.-H. Cheng, Growth of Mn_5Ge_3 ultrathin film on Ge(111), Chin. Phys. Soc. 17 (2008) 3902-3905.

[12] A. Portavoce, O. Abbes, A. Spiesser, C. Girardeaux, L. Michez, V. Le Thanh, Mn–Ge nanocluster formation vs. diluted magnetic semiconductor formation, Scripta Mater. 100 (2015) 70-73.

[13] S. Zhou, W. Zhang, A. Shalimov, Y. Wang, Z. Huang, D. Buerger, A. Mücklich, W. Zhang, H. Schmidt and M. Helm, Magnetic Mn_5Ge_3 nanocrystals embedded in crystalline Ge: a magnet/semiconductor hybrid synthesized by ion implantation, Nanoscale Res. Lett. 7 (2012) 528.

[14] A. Spiesser, F. Virot, L.-A. Michez, R. Hayn, S. Bertaina, L. Favre, M. Petit, V. Le Thanh, Magnetic anisotropy in epitaxial Mn_5Ge_3 films, Phys. Rev. B 86 (2012) 035211.

[15] A. Spiesser, S.F. Olive-Mendez, M.-T. Dau, L.A. Michez, A. Watanabe, V. Le Thanh, A. Glachant, J. Derrien, A. Barski, M. Jamet, Effect of thickness on structural and magnetic

properties of Mn_5Ge_3 films grown on Ge(111) by solid phase epitaxy, Thin Solid Films 518 (2010) S113–S117.

[16] L.-A. Michez, F. Virot, M. Petit, R. Hayn, L. Notin, O. Fruchart, V. Heresanu, M. Jamet, V. Le Thanh, Magnetic anisotropy and magnetic domain structure in C-doped Mn_5Ge_3, J. Appl. Phys. 118 (2015) 043906.

[17] L.-A. Michez, A. Spiesser, M. Petit, S. Bertaina, J.-F. Jacquot, D. Dufeu, C. Coudreau, M. Jamet, V Le Thanh, Magnetic reversal in Mn_5Ge_3 thin films: An extensive study, J. Phys.: Condens. Matter 27 (2015) 266001.

[18] A. Spiesser, I. Slipukhina, M.-T. Dau, E. Arras, V. Le Thanh, L. Michez, P. Pochet, H. Saito, S. Yuasa, M. Jamet, J. Derrien, Control of magnetic properties of epitaxial $Mn_5Ge_3C_x$ films induced by carbon doping, Phys. Rev. B 84 (2011) 165203.

[19] S.F. Olive-Méndez, L.A. Michez, A. Spiesser, V. Le Thanh, Epitaxial growth of strained Mn_5Ge_3 nanoislands on Ge(001), Phys. Status Solidi (B) 252 (2015) 854–1859.

[20] H. Kim, G.-E Jung, J.-H. Lim, K.H. Chung, S.-J. Kahng, W.-j. Son, S. Han, Epitaxial Mn_5Ge_3 nano-islands on a Ge(001) surface, Nanotechnology 19 (2008) 025707.

[21] D.D. Dang, O. Dorj, V. Le Thanh, C.H. Soon, C. Sunglae, Strain-induced modification in the magnetic properties of Mn_5Ge_3 thin films, J. Appl. Phys. 114 (2013) 073906.

[22] C. Sürgers, K. Potzger, G. Fischer, Magnetism of carbon doped Mn_5Si_3 and Mn_5Ge_3 films, J. Chem. Sci. 121 (2009) 173-176.

[23] N. Stojilovic, S.V. Dordevic, R. Hu, C. Petrovic, Effect of carbon doping on electronic transitions in Mn_5Ge_3, J. Appl. Phys. 114 (2013) 053708.

[24] M. Gajdzik, C. Sürgers, M.T. Kelemen, H.v. Löhneysen, Strongly enhanced Curie temperature in carbon-doped Mn_5Ge_3 films, J. Magn. Magn. Mater. 221 (2000) 248-254.

[25] A. Spiesser, V. Le Thanh, S. Bertaina, L.A. Michez, Thermal stability of epitaxial Mn_5Ge_3 and carbon-doped Mn_5Ge_3 films, Appl. Phys. Lett. 99 (2011) 121904.

[26] M.-T. Dau, V. Le Thanh, T.-G. Le, A. Spiesser, M. Petit, L.A. Michez, R. Daineche, Mn segregation in Ge/Mn_5Ge_3 heterostructures: The role of surface carbon Adsorption, Appl. Phys. Lett. 99 (2011) 151908.

[27] A. Hammersley, FIT2D: a multi-purpose data reduction, analysis and visualization program. J. Appl. Crystallogr. 49(2) (2016) 646-652.
http://www.esrf.fr/computing/scientific/FIT2D/

[28] V.G. Myagkov, L.E. Bykova, A.A. Matsynin, M.N. Volochaev, V.S. Zhigalov, I.A. Tambasov, Y. Lu. Mikhlinb, D.A. Velikanov, G.N. Bondarenkob, Solid state synthesis of Mn_5Ge_3 in Ge/Ag/Mn trilayers: Structural and magnetic studies, J. Solid State Chem. 246 (2017) 379–387.

[29] A. Alvídrez-Lechuga, R. López Antón, J.T. Holguín-Momaca, F. Espinosa-Magaña, S.F. Olive-Méndez, Role of the substrate temperature on the growth of Mn_5Ge_3 thin films by co-deposition of Mn and Ge on Ge(001) substrates by magnetron sputtering, Thin Solid Films 616 (2016) 111–115.

[30] R. T. Lechner, V. Holý, S. Ahlers, D. Bougeard, J. Stangl, A. Trampert, A. Navarro-Quezada, G. Bauer. Self-assembled Mn_5Ge_3 nanomagnets are close to the surface and deep inside a $Ge_{1-x}Mn_x$ epilayer, Appl. Phys. Lett. 95 (2009) 023102.

[31] H. Kim, G.-E. Jung, J. K. Yoon, K.H. Chung, S-J. Kahng, Surface atomic structure of alloyed Mn_5Ge_3 (0001) by scanning tunneling microscopy, Surf. Sci. 602 (2008) 481-486.

[32] A. Bihler, C. Jaeger, T. Vallaitis, M. Gjukic, M. S. Brandt, E. Pippel, J. Woltersdorf, U. Gösele, Structural and magnetic properties of Mn_5Ge_3 clusters in a dilute magnetic germanium matrix, Appl. Phys. Lett. 88 (2006) 112506.

[33] P.A. Bennett, Z. He, D.J. Smith, F.M. Ross, Endotaxial silicide nanowires: A review, Thin Solid Films 519 (2011) 8434–8440.

[34] E. Arras, F. Lançon, I. Slipukhina, É. Prestat, M. Rovezzi, S. Tardif, A. Titov, P. Bayle-Guillemaud, F. d'Acapito, A. Barski, V. Favre-Nicolin, M. Jamet, J. Cibert, and P. Pochet, Interface-driven phase separation in multifunctional materials: The case of the ferromagnetic semiconductor GeMn, Phys. Rev. B 85 (2012)115204.

[35] R. M. Gutiérrez-Pérez, R. López Antón, K. Załęski, J. T. Holguín-Momaca, F. Espinosa-Magaña, S. F. Olive-Méndez, Tailoring magnetization and anisotropy of tetragonal Mn_3Ga thin films by strain-induced growth and spin orbit coupling, Intermetallics 92 (2018) 20–24.

[36] R. Zhang, M. Liu, L. Lu, S.-B. Mi and H. Wang, Strain-tunable magnetic properties of epitaxial lithium ferrite thin film on $MgAl_2O_4$ substrates, J. Mater. Chem. C 3 (2015) 5598-5602.

[37] M. D. Kuz'min, Shape of temperature dependence of spontaneous magnetization of ferromagnets: quantitative analysis, Phys. Rev. Lett. 94 (2005) 107204.